

Multiwavelength Observations of the Black Hole X-ray Binary MAXI J1820+070 in the Rebrightening Phase

Tomohiro YOSHITAKE¹, Megumi SHIDATSU², Yoshihiro UEDA¹, Shin MINESHIGE¹, Katsuhiro L. MURATA³, Ryo ADACHI³, Hiroyuki MAEHARA^{4,5}, Daisaku NOGAMI¹, Hitoshi NEGORO⁶, Nobuyuki KAWAI³, Masafumi NIWANO³, Ryohei HOSOKAWA³, Tomoki SAITO⁷, Yumiko OASA^{8,9}, Takuya TAKARADA^{9,10}, Takumi SHIGEYOSHI⁸ and OISTER Collaboration

¹Department of Astronomy, Kyoto University, Kitashirakawa-Oiwake-cho, Sakyo-ku, Kyoto, Kyoto 606-8502, Japan

²Department of Physics, Ehime University, 2-5, Bunkyocho, Matsuyama, Ehime 790-8577, Japan

³Department of Physics, Tokyo Institute of Technology, 2-12-1 Ookayama, Meguro-ku, Tokyo 152-8551, Japan

⁴Okayama Observatory, Kyoto University, 3037-5 Honjo, Kamogatacho, Asakuchi, Okayama 719-0232, Japan

⁵Subaru Telescope Okayama Branch Office, National Astronomical Observatory of Japan, National Institutes of Natural Sciences, 3037-5 Honjo, Kamogata, Asakuchi, Okayama 719-0232, Japan

⁶Department of Physics, Nihon University, 1-8-14 Kanda-Surugadai, Chiyoda-ku, Tokyo 101-8308, Japan

⁷Nishi-Harima Astronomical Observatory, Center for Astronomy, University of Hyogo, 407-2 Nishigaichi, Sayo-cho, Sayo, Hyogo 679-5313, Japan

⁸Faculty of education, Saitama University, Simo-okubo 255, Sakura-ku, Saitama 338-8570, Japan

⁹Graduate School of Science and Engineering, Saitama University, Simo-okubo 255, Sakura-ku, Saitama 338-8570, Japan

¹⁰Astrobiology Center, NINS, 2-21-1 Osawa, Mitaka, Tokyo 181-8588, Japan

*E-mail: yoshitake@kusastro.kyoto-u.ac.jp

Received (reception date); Accepted (acceptation date)

Abstract

We report the results of quasi-simultaneous multiwavelength (near-infrared, optical, UV, and X-ray) observations of the Galactic X-ray black hole binary MAXI J1820+070 performed in 2019 May 10–13, ~ 60 days after the onset of the first rebrightening phase. It showed a much larger optical-to-X-ray luminosity ratio (~ 8) than in the initial outburst epoch. The primary components of the spectral energy distribution (SED) can be best interpreted by radiatively inefficient accretion flow (RIAF) spectrum showing a luminosity peak in the optical band. By comparison with theoretical calculations, we estimate the mass accretion rate to be $\dot{M}/(8L_{\text{Edd}}/c^2) \sim 10^{-3}$, where c is the light speed and L_{Edd} is the Eddington luminosity. In addition to the RIAF emission, a blue power-law component is detected in the optical-UV SED, which is most likely

synchrotron radiation from the jet. The optical spectrum taken at the Seimei telescope shows a weak and narrow $H\alpha$ emission line, whose emitting region is constrained to be $\gtrsim 2 \times 10^4$ times the gravitational radius. We suggest that the entire disk structure cannot be described by a single RIAF solution but cooler material responsible for the $H\alpha$ emission must exist at the outermost region.

Key words: X-rays: individual (MAXI J1820+070) — X-rays: binaries — accretion, accretion disks — black hole physics

1 Introduction

A Galactic black hole X-ray binary (BHXB), consisting of a stellar-mass black hole and a companion star, is an ideal object to study accretion physics. Most of the known BHXBs are transient sources; While usually in a faint, dormant state, they can suddenly brighten by several orders of magnitudes during recurring outburst periods. In their outbursts they show several different states with distinct spectral and timing properties (for a review, see e.g., Done et al. 2007, Tetarenko et al. 2016). At low luminosities, they stay in the low/hard state (LHS), which is characterized by a strong short-term variation typically on timescales of ~ 0.1 – 10 s and a hard, power-law shaped spectrum often with an exponential cutoff at ~ 100 keV. When the luminosity increases, they make a transition to the so-called high/soft state (HSS), where the spectrum is well represented by the Multi-color Disk (MCD) model (Mitsuda et al. 1984), an approximated spectral model of the standard accretion disk (Shakura & Sunyaev 1973), and the short-term variation is strongly suppressed.

An important issue in understanding black-hole accretion flow is how the standard disk forms and evolves with the mass accretion rate. The standard disk is believed to extend down to the innermost stable circular orbit (ISCO) in the HSS, because the observed r_{in} value of a BHXB is found to be constant over a wide range of the disk luminosity L_{disk} (e.g., Ebisawa et al. 1993). By contrast, many studies suggest that the accretion disk in the LHS is truncated before reaching the ISCO (e.g., Makishima et al. 2008; Tomsick et al. 2009; Shidatsu et al. 2011; Shidatsu et al. 2013) and the inner part is replaced by low-density hot flow that is responsible for the Comptonization. These results basically agree with a prediction from a standard theoretical model of black hole accretion flows (e.g., Esin et al. 1997): when the mass accretion rate becomes sufficiently small (typically smaller than ~ 0.1 times the Eddington rate), the standard disk is truncated and its inner region becomes radiatively inefficient accretion flow (RIAF). The model also predicts that the truncation radius increases as the mass accretion rate decreases. However, detailed observational studies of the disk structure in the LHS have been limited to relatively high X-ray luminosities above $\sim 10^{36}$ erg s $^{-1}$ and hence at which luminosity the standard disk is generated is unknown. To answer

this question, it is important to observe BHXBs in the very dim periods.

MAXI J1820+070 (hereafter MAXI J1820) is a Galactic BHXB discovered with Monitor of All-sky X-ray Image (MAXI; Matsuoka et al. 2009) on 2018 March 11 (Kawamuro et al. 2018). Soon after the discovery, the X-ray source was identified with the optical variable source ASSASN-2018ey (Tucker et al. 2018; Denisenko 2018), thanks to the refined position by *Swift* follow-up observations. The X-ray flux exceeded 1 Crab in the 2–20 keV band at the peak (Shidatsu et al. 2018). The high X-ray flux during the outburst, the small distance (3 kpc; Gandhi et al. 2019), and low Galactic absorption (with a hydrogen column density of $N_{\text{H}} \sim 10^{21}$ cm $^{-2}$) of the source enabled extensive observations in various wavelengths (Shidatsu et al. 2018, Tucker et al. 2018 for discovery and monitoring early outburst periods; e.g., Buisson et al. 2019, You et al. 2021 for X-ray spectral studies; e.g., Paice et al. 2019, Ma et al. 2021 for short-term variability; e.g., Sánchez-Sierras & Muñoz-Darias 2020, Torres et al. 2019a for optical or near-infrared spectroscopy; Veledina et al. 2019, Poutanen et al. 2022 for polarimetry, e.g., Bright et al. 2020, Atri et al. 2020 for radio observations, e.g., Shidatsu et al. 2019, Tetarenko et al. 2021, Shaw et al. 2021 for multi-wavelength studies).

After the initial outburst that lasted for ~ 200 days, MAXI J1820 has shown several rebrightenings in the optical and X-ray bands. In these phases, the optical-to-X-ray luminosity ratio was found to be very large, however, compared with that in the initial outburst epoch. This suggests that the accretion disk structure may be very different from the normal LHS or HSS observed in the 2018 outburst. In this article, we investigate the properties of the accretion flow in MAXI J1820 on the basis of our quasi-simultaneous multi-wavelength observations performed around 2019 May 11, which corresponds to the decay phase in the first rebrightening. We assume a black hole mass of $M = 7$ – $8 M_{\odot}$ and an inclination angle of $i = 69^{\circ}$ – 77° , respectively, which are estimated by Torres et al. (2019a), and $D = 3$ kpc (Gandhi et al. 2019).

2 Observations and Data Reduction

We observed MAXI J1820 with Swift/XRT (X-ray), Swift/UVOT (UV), and OISTER (near-infrared to optical) on 2019 May 10–13. Optical spectroscopic observations were performed with KOOLS-IFU on Seimei telescope on 2019 May 11. Table 1 summarizes the observation log.

2.1 Swift

The time-averaged Swift/XRT spectrum was obtained via the XRT on-demand web interface¹. Here, we combined all the XRT data taken from 2019 May 10–13 (OBSIDs=00010627169, 00010627171, 00010627172, and 00010627173) to improve statistics. The Swift/UVOT data taken on 2019 May 11 were analyzed by using HEASoft version 6.26.1 and the latest Swift/UVOT Calibration Database (CALDB) as of 2018 April. We started with the cleaned sky-coordinate images of the individual filters: UVW1, UVW2, UVM2, and U bands. We performed aperture photometry using the UVOT-specific tool `uvot2pha` included in HEASoft, where we defined the source region as a circle with a 5" radius centered at the source position and the background region as a circle of a 20" radius in a blank-sky area.

2.2 Seimei Telescope

The 3.8-m Seimei telescope of Kyoto University is a new telescope at the Okayama Observatory (Craine 2010). The Kyoto Okayama Optical Low-dispersion Spectrograph with an integral field unit (KOOLS-IFU; (Yoshida 2005; Matsubayashi et al. 2019)) is installed there through the optical fibers. The data were taken under the program 19A-K-0009. We used the VPH-blue grism, whose wavelength coverage is 4000–8900 Å and wavelength resolution is $R = \lambda/\Delta\lambda \sim 500$.

We adopted the standard data reduction procedures for optical spectra: overscan and bias subtraction, flat fielding, wavelength calibration, spectral extraction, sky subtraction, and flux calibration, utilizing the Hydra package in IRAF (Craine 1994; Barden 1995) and a python script specifically developed for KOOLS-IFU data reduction². We used arc lamp (Hg and Ne) data for the wavelength calibration. The sky subtraction was performed by using the object frames themselves. The sky brightness was estimated with the fibers placed on blank-sky regions. These processes were carried out for the individual object frames. We made the final spectrum through median combination of the spectra made from the individual object frames. As the flux error in each spectral bin, we adopted the standard deviation of the fluxes in the line-free region around the H α

line (6300–6500 Å and 6600–6800 Å), which was estimated to be 1.4×10^{-17} erg cm⁻² s.

Analysis of the Seimei spectrum was carried out with XSPEC. Conversion of the spectral data to the XSPEC format was performed with the ftool `ftf1x2xsp`. To consider the spectral resolution of the Seimei/KOOLS-IFU, we created, using the ftool `ftgenrsp`, a response matrix file such that the response is expressed as a Gaussian for each wavelength bin. A full width at half maximum (FWHM) of 9.55 Å was adopted for the Gaussian components, which was estimated from the profile of a Ne line around the H α line in the arc lamp frame.

2.3 OISTER

The Optical and Infrared Synergetic Telescopes for Education and Research (OISTER) is a framework of multi-band imaging observations based on a Target-of-Opportunity (ToO) program. Many small-to-medium size telescopes operated by observatories and Universities in Japan participate in the OISTER collaboration, including the Multicolor Imaging Telescopes for Survey and Monstrous Explosions (MITSuME) at the Akeno Observatory (Kotani et al. 2005; Yatsu et al. 2007; Shimokawabe et al. 2008) and at the Okayama Observatory (Yanagisawa et al. 2010), 55 cm SaCRA telescope at Saitama University (Oasa et al. 2020), and the 2.0 m Nayuta telescope at the Nishi-Harima Astronomical Observatory (Ishiguro et al. 2011; Takahashi et al. 2013).

The OISTER optical and near-infrared data were reduced on IRAF by following standard procedures including bias and dark subtraction, flat fielding, and bad pixel masking. IRAF was also used for photometry. The magnitudes of MAXI J1820 were calibrated with nearby reference stars, whose magnitudes were taken from the UCAC4 catalog (Zacharias et al. 2013) and Pan-STARRS1 Surveys (Chambers et al. 2016) for the optical data, and the Two Micron All Sky Survey Point Source Catalog (Cutri et al. 2003) for the near-IR data. Their typical errors were estimated as $\sim 10\%$ of the magnitudes.

3 Analysis and Results

3.1 Long-term Light Curves

Fig. 1 shows the long-term X-ray and optical light curve over three years since its discovery. The X-ray light curve was made from the MAXI/Gas Slit Camera (GSC; Mihara et al. 2011) data via the MAXI on-demand web interface (Nakahira et al. 2013)³. The optical data were taken by the OISTER collaboration (Adachi et al. in prep). The X-ray (2–10 keV) peak flux in rebrightenings were ~ 1 order of magnitude lower than that in the 2018 outburst, whereas the optical peak fluxes in these activities were comparable. Our multi-wavelength observation

¹ https://www.swift.ac.uk/user_objects/

² http://www.kusastro.kyoto-u.ac.jp/~kazuya/p-kools/reduction-201806/install_software.html

³ <http://maxi.riken.jp/mxondem>

Table 1. Observation Log

Observatory/Instrument (Filters))	Date	Exposure (ks)	Observation ID
Swift/XRT	2019 May 10–13	4	10627169/171/172/173
Swift/UVOT (UVM2, U, UVW1, UVW2)	2019 May 11	0.1 each	10627171
OISTER (grizJHK)	2019 May 12		
Seimei/KOOLS-IFU	2019 May 11	0.6 ($\times 15$ frames)	

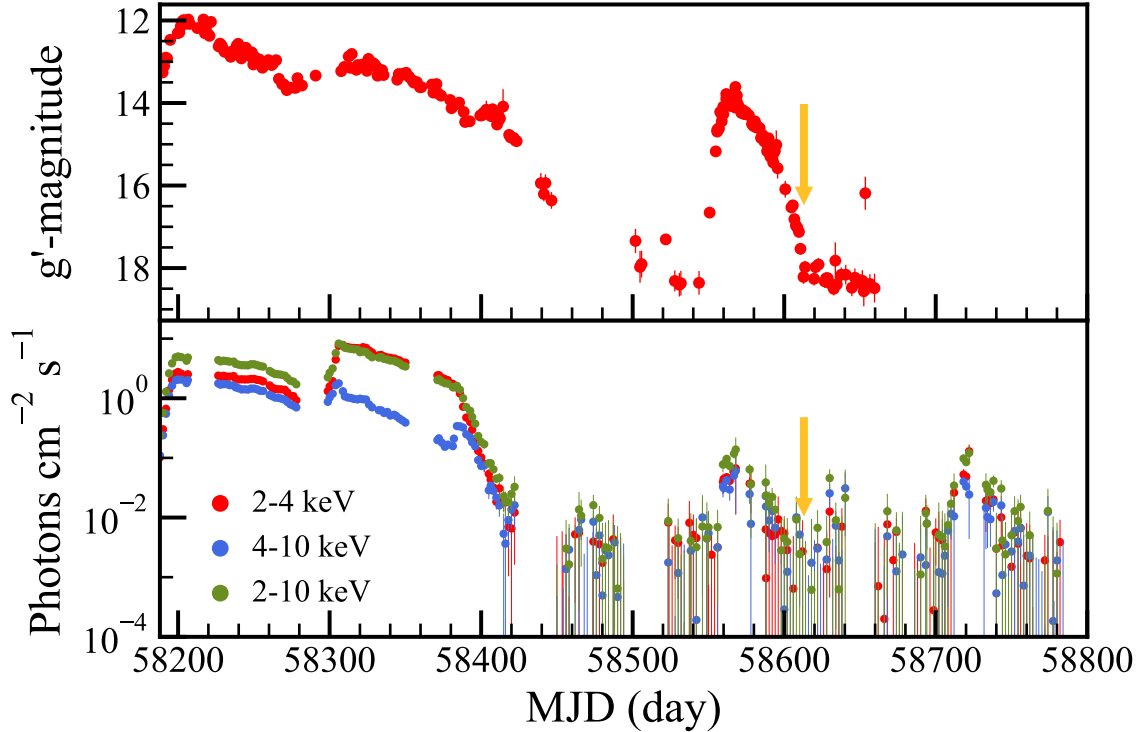


Fig. 1. (Top) g' -band optical light curve of MAXI J1820 from the OISTER collaboration (Adachi et al. in prep). (Bottom) X-ray light curve in 2–10 keV from the MAXI/GSC. MJD 58200 corresponds to 2019 March 23. The yellow line presents our observation epoch (2019 May 11 = MJD 58614).

was performed in the last part of the decay phase of the first rebrightening, with the g' -band magnitude of ~ 16 mag.

3.2 Multi-wavelength SED

Figure 2 shows the multi-wavelength data from the X-ray to near-infrared bands. We analyzed the data on XSPEC version 12.11.1. In the analysis, we adopted χ^2 statistics for the infrared to UV data, whereas C-statistics for the X-ray data because of the low data statistics. The errors represent the 90% confidence range for one parameter, unless otherwise stated. We adopted the solar abundance table given by Wilms et al. (2000).

3.2.1 X-ray Spectrum

We first focused on the X-ray spectrum. The origin of the X-ray emission from BHXBs at such dim phases is still unclear, although several possible scenarios are proposed, including the Bremsstrahlung radiation and/or Comptonization in the RIAF (e.g., Manmoto et al. 1997), or synchrotron or Comptonization in the jet (e.g., Markoff et al. 2001). Here, we adopted an

empirical model: the simple power-law model, often used to characterize the LHS spectra. To account for the interstellar absorption, the TBabs model was multiplied with N_{H} fixed at $1.1 \times 10^{21} \text{ cm}^{-2}$ (Uttley et al. 2018).

The model successfully reproduced the X-ray spectrum. Figure 2 plots the data and the best-fit model spectrum, and Table 2 gives the best-fit parameters.

3.2.2 Infrared to UV SED

Next, we analyzed the SED in the near-infrared (NIR), optical, and UV bands. The photons in these wavelengths from BHXBs can be produced in the outer region of the accretion disk, in the jets, and on the surface of the companion star. We considered two possibilities as the primary origin of the SED: (1) RIAF and (2) truncated hot standard disk (hereafter we call Model 1 and 2, respectively) and fit the SED with models based on these two cases in the following sections.

In both cases, to consider the blackbody emission from the companion star, we added `bbodyrad`, whose parameters are the temperature T_{bb} and the normalisation, which is determined

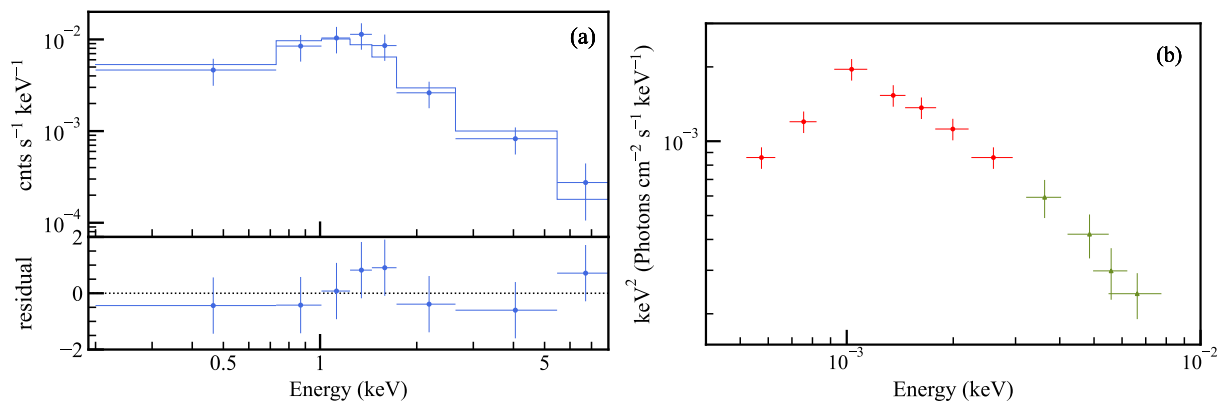


Fig. 2. (a) folded (instrumental response included) X-ray spectrum with the best-fit absorbed power-law model (top) and the residuals (bottom). (b) infrared to UV SED where extinction is not corrected.

by the radius of the emission region. The companion star of MAXI J1820 is suggested to be a K4V star (Torres et al. 2019b), whose surface temperature is ~ 4700 K. Hence, we fixed T_{bb} at 4700 K, and assumed a typical stellar radius of $0.65 R_{\odot}$ for a K4V star in this analysis. Note that this component turned out not to be significant in either case (see below), but since it should certainly exist, we included it to describe the actual physical condition. The interstellar extinction was also taken into account by incorporating the `redden` model with $E(B - V)$ at 0.16 (Baglio et al. 2018). Thus, Model 1 and 2 were expressed as `redden*(cutoffpl+bbbodyrad)` and `redden*(diskbb+bbbodyrad)`, respectively.

3.2.3 Model 1: RIAF

Theoretical studies suggest that the synchro-cyclotron emission of thermal electrons in the RIAF is dominant and the spectrum peaks around the NIR to UV band (Manmoto et al. 1997). As an approximated model for the synchro-cyclotron spectrum, we adopted the cutoff power-law model `cutoffpl`, whose parameters are the photon index Γ and the cutoff energy E_{cut} . The former parameter was fixed at -0.232 , which was estimated from Figure 8 in Manmoto et al. (1997).

This model, however, underestimated the observed flux and left large residuals in the UV band, as shown in Figure 3. They gave a large χ^2 value, 59.2, with the degree of freedom (d.o.f.) of 9. This suggests that additional emission components, such as the jet synchrotron emission and Comptonization components in the RIAF, are required. To account for these components, a power-law component was added to both models. The final SED model was then expressed as `redden*(cutoffpl+powerlaw+bbbodyrad)`. This model was found to improve the fit significantly, yielding $\chi^2 = 9.9$ with the d.o.f. reduced by 2.

The model successfully reproduces the actual SED profile. The best-fit model and its parameters are shown in Figure 3 and Table 2, respectively. The best-fit `cutoffpl` component

indicates that the synchro-cyclotron spectrum from RIAF has a peak at $E_{\text{cut}} = 6.0_{-0.6}^{+1.0} \times 10^{-4}$ keV.

3.2.4 Model 2: Truncated Hot Standard Disk

In Model 2, we assumed the standard disk emission dominates the NIR to UV flux, for which we used the MCD model (the `diskbb` model on XSPEC (Mitsuda et al. 1984)). Its parameters are the inner disk temperature T_{in} and the normalization, which is related to the inner disk radius R_{in} . As in Model 1, this model underestimated the UV flux (Fig. 4), yielding a large χ^2 value of 45.7, with d.o.f. = 9. We then combined an additional power-law component and adopted the model `redden*(diskbb+powerlaw+bbbodyrad)`.

This model improved the fit and reproduced the SED equally well compared with Model 1, giving $\chi^2 = 11.4$ with a decrease in d.o.f. by 2. The best-fit model is shown in Figure 4 and the resultant parameters are listed in Table 2. We obtained $T_{\text{in}} \approx 5.9 \times 10^{-4}$ keV (i.e., $\approx 6.8 \times 10^3$ K) and $R_{\text{in}} \approx 6.3 \times 10^5$ km. This suggests that the standard disk was highly truncated and replaced by the RIAF inside it.

BHXBs often show significant irradiation of X-rays on the outer disk region in their outburst periods. To investigate the effects by the X-ray illumination in the infrared to UV band, we tested an irradiated disk model. Here, we only considered the illumination by the inner disk emission and ignored that by the jet emission, which would cause only a limited effect due to the relativistic beaming. According to Miller-Jones et al. (2006), jets in BHXBs typically have a bulk Lorentz factor of $\Gamma_{\text{jet}} \gtrsim 10$. Considering the luminosity is proportional to δ^4 , where δ is the beaming factor expressed with the angle θ from the jet axis as $\delta = \Gamma_{\text{jet}}^{-1}(1 - \beta \cos \theta)^{-1}$, we found that the flux of the jet emission illuminating the outer disk (at $\theta \gtrsim 90^\circ$) was smaller by a factor of $\gtrsim 5$ than that for the observers at $\theta \sim 70^\circ$.

We employed the irradiated disk model `diskir` (Gierliński et al. 2008; Gierliński et al. 2009) and replaced the `diskbb` model in Model 2 with it to fit the SED. The `diskir` model

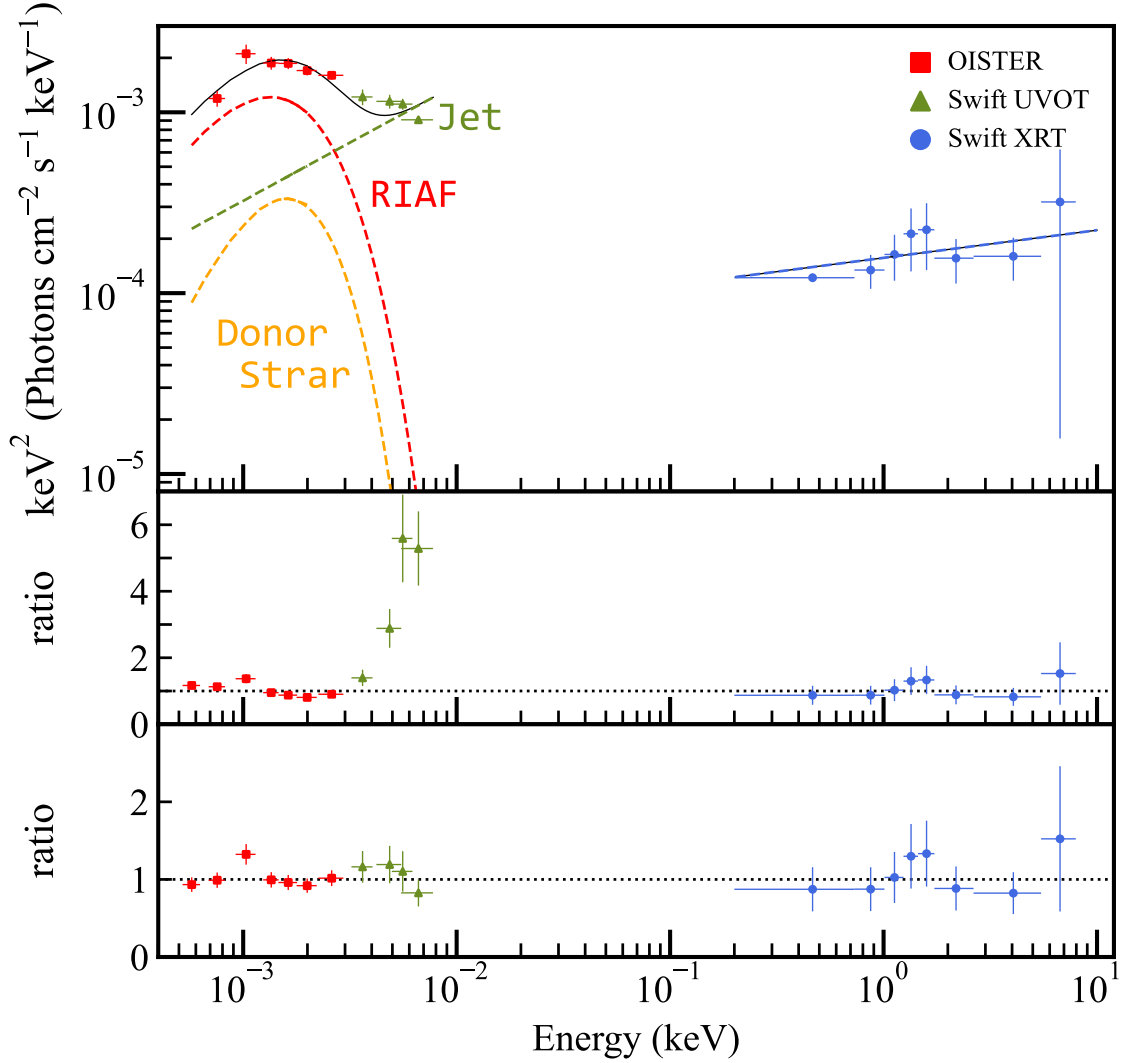


Fig. 3. Top: the SED data with the best-fit $\text{redden}*(\text{powerlaw}+\text{cutoffpl}+\text{bbodyrad})$ model (Model 1) in the NIR to UV band and the unfolded spectrum with the best-fit $\text{TBabs}*\text{power-law}$ model (Section 3.2.1) in X-rays, all corrected for the interstellar absorption and extinction. The individual components are separately plotted. Middle: the data versus model ratio of the $\text{redden}*(\text{cutoffpl}+\text{bbodyrad})$ model (in the infrared to UV band) and the $\text{TBabs}*\text{power-law}$ model (in the X-ray band). Bottom: Same as the middle panel, but with the $\text{redden}*(\text{powerlaw}+\text{cutoffpl}+\text{bbodyrad})$ model in the infrared to UV band.

calculates an irradiated disk spectrum, where the X-ray photons are produced by the MCD emission and its Comptonization. Here, we ignored the illumination of the inner disk region (i.e., $f_{\text{in}} = 0$, where f_{in} is the fraction of the luminosity of the Comptonization component that is thermalized in the inner disk), and fixed T_e at 100 keV, f_{out} at 0.01, and $\log(R_{\text{out}}/R_{\text{in}})$ at 0.69 (where T_e , f_{out} , and R_{out} are the electron temperature of the Comptonization component, the fraction of the bolometric flux which is thermalized in the outer disk, and the outer disk radius, respectively). We note that the fit results unchanged when $f_{\text{out}} = 0.1$ and 0.001 were adopted. For R_{out} , we employed the Roche lobe size of the black hole, 3.2×10^6 km, which was calculated from Equation (4) in Paczyński (1971a), while we assumed $R_{\text{in}} = 6.3 \times 10^4$ km, which was estimated from the normalization of the best-fit diskbb model. The other parameters:

the inner disk temperature T_{in} , the photon index Γ , the luminosity ratio L_c/L_d (where L_c and L_d represents the luminosity of the Comptonization and disk components, respectively), and the normalization, whose definition is the same as that of diskbb , were allowed to vary.

The resultant parameters, however, unchanged from the best-fit diskbb model within the 90% confidence ranges, suggesting that X-ray irradiation makes only a negligible effect to the infrared to UV continuum. From this model, we obtained $T_{\text{in}} = 5.9_{-0.7}^{+1.2} \times 10^{-4}$ keV, $\Gamma = 1.9_{-0.3}^{+0.4}$, $L_c/L_d = 1.1_{-0.2}^{+1.2}$, and the normalization of $(2 \pm 1) \times 10^{12}$, which corresponds to $R_{\text{in}} = (7 \pm 2) \times 10^5 (D/3 \text{ kpc}) (\cos i / \cos 70^\circ)^{-1/2}$ km.

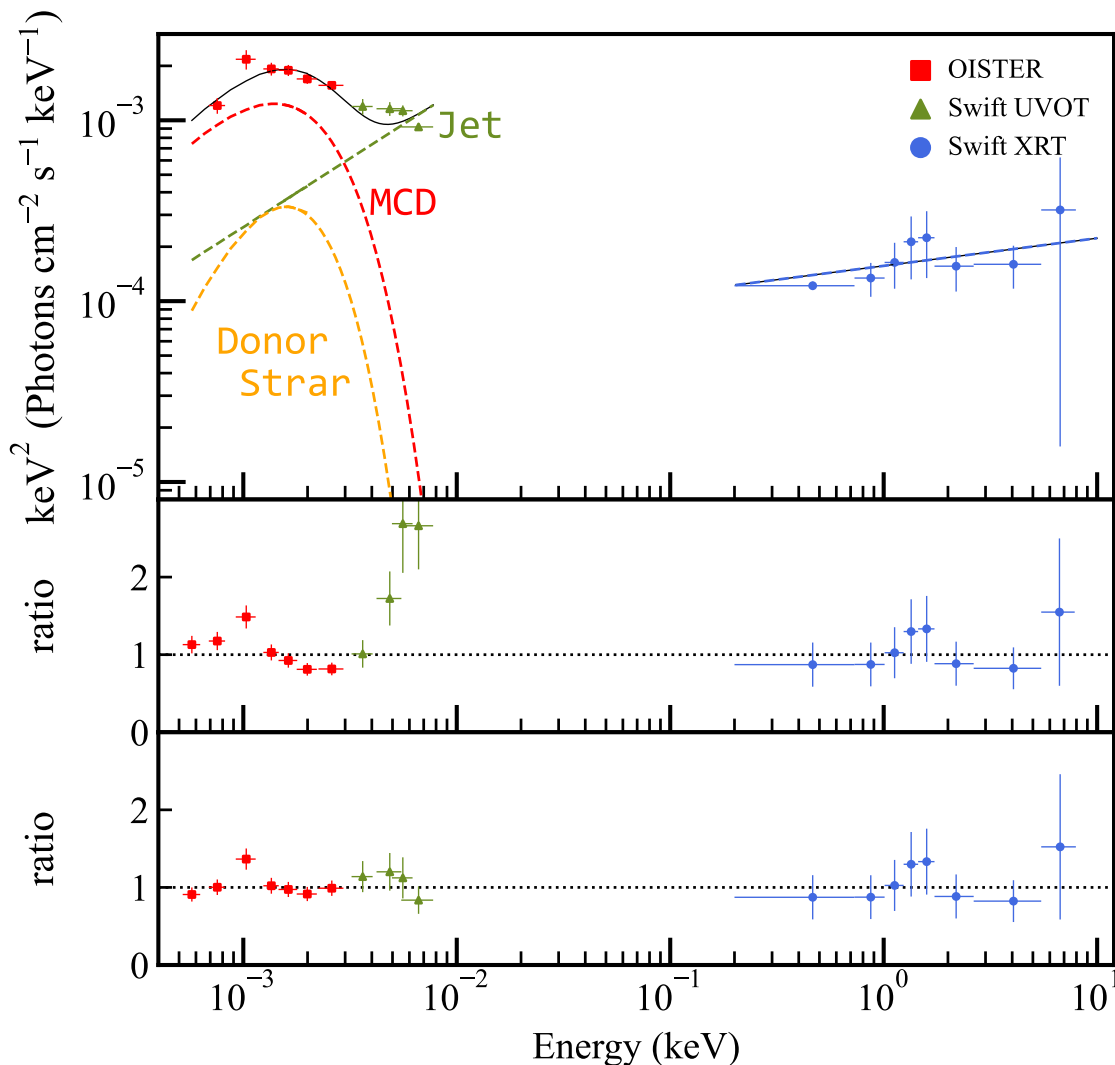


Fig. 4. Same as Fig. 3, but for the `redden*(diskbb+bbbodyrad)` model in the middle panel and for the `redden*(powerlaw+diskbb+bbbodyrad)` model (Model 2) in the top and bottom panels, in the NIR to UV band.

3.3 Optical Spectrum

Figure 5 shows the Seimei spectrum of MAXI J1820. The source signals are significantly detected over 5000–7000 Å, in which the H α emission line (6563 Å) is clearly seen.

We performed spectral fitting on XSPEC, adopting the data around the H α line in a wavelength range of 6300–6700 Å. First, we applied a single Gaussian and a power-law model for the line and the continuum, respectively. The spectral model gave an acceptable fit, yielding $\chi^2/\text{d.o.f} = 72/137$ and a line-center wavelength of 6565 ± 3 Å and a 1-sigma line width of 11 ± 4 Å. Next, we replaced the single Gaussian with a double Gaussian at different energies. This model is often used to approximately represent the profile of a line emitted from an accretion disk (e.g., Tetarenko et al. 2021). The best-fit model ($\chi^2/\text{d.o.f}=67/134$) gave the double-peak separation of 14 Å, FWHM of 20 Å and the half width at zero intensity (HWZI)

of 19 Å, where the zero intensity was measured at 5σ level of a Gaussian. It is possible to roughly estimate the innermost radius at which the line is emitted as $R_{\text{in}} = (c \sin(i)/v_{\text{in}})^2 r_g$, where c is the light velocity, i the inclination, v_{in} the velocity at the inner edge of the disk, and $r_g \equiv GM/c^2$ (G is the gravitational constant) the gravitational radius (see Bernardini et al. 2016). Using the HWZI value obtained from the double Gaussian model to estimate v_{in} , we obtained $R_{\text{in}} = 1.0 \times 10^5 r_g$ for $i = 70^\circ$.

Finally, to most accurately estimate the line emitting radii directly from the data, we apply a physical disk emission line model, `diskline`, in place of the Gaussian models. The `diskline` model computes the emission line from the accretion disk illuminated by the X-rays emitted in the inner disk region, with input parameters of the line energy, the inner and outer disk radii of the emission region (R_{in} and R_{out} , respectively), the

Table 2. Best-fit parameters of the X-ray spectrum and the NIR to UV SED

Component	Parameter	Unit	Value		
			X-ray*	NIR–UV (Model 1) [†]	NIR–UV (Model 2) [†]
powerlaw	Γ		1.8 ± 0.3	$1.4^{+0.4}_{-0.9}$	$1.2^{+0.5}_{-1.2}$
	Flux	10^{-12} ergs cm ⁻² s ⁻¹	$6.3^{+1.4}_{-1.3} \times 10^{-1}$	$1.8^{+0.9}_{-1.0}$	1.5 ± 1.0
	$L_{\text{pow}}^{\text{X,opt}\ddagger}$	erg s ⁻¹	6×10^{32}	2×10^{33}	2×10^{33}
cutoffpl	Γ		-	-0.232 (fixed)	-
	E_{cut}	keV	-	$6.0^{+1.0}_{-0.6} \times 10^{-4}$	-
	norm		-	$3.0^{+1.1}_{-1.5} \times 10^4$	-
	$L_{\text{cpl}}^{\ddagger}$	erg s ⁻¹	-	3×10^{33}	-
diskbb	T_{in}	keV	-	-	$5.9^{+1.0}_{-0.7} \times 10^{-4}$
	$R_{\text{in,SED}}^{\S}$	km	-	-	$6.3^{+1.7}_{-2.3} \times 10^5$
	$L_{\text{dbb}}^{\ddagger}$	erg s ⁻¹	-	-	3×10^{33}
C-stat/d.o.f., $\chi^2/\text{d.o.f.}^{\ddagger}$			60/154	9.9/7	11.4/7

* TBabs*powerlaw, with N_{H} of TBabs fixed at 1.1×10^{21} cm⁻².

[†] reddens*(cutoffpl+powerlaw+bbbodyrad) (Model 1) and reddens*(diskbb+powerlaw+bbbodyrad) (Model 2), with $E(B - V)$ of reddens fixed at 0.16. For the bbbodyrad component, $T_{\text{bb}} = 4700$ K and $R_{\text{bb}} = 0.65 R_{\odot}$, and $D = 3$ kpc were assumed.

[‡] Absorption/extinction corrected luminosity of each component in 0.5–5 keV (for the X-ray data) and 0.5–5 eV (for the NIR–UV data). In calculating the luminosity of the diskbb component, $D = 3$ kpc and $i = 70^\circ$ are assumed. [§] $D = 3$ kpc, $i = 70^\circ$, and $M = 7 M_{\odot}$ are assumed.

[#] Cash statistics was used for the X-ray spectrum, whereas χ^2 statistics for the NIR to UV SED. Here, C-stat/d.o.f. and $\chi^2/\text{d.o.f.}$ are shown for the results from the former and latter data, respectively.

inclination angle (i), and the power law index (α) of emissivity law ($\propto E^\alpha$). We adopted $\alpha = -3$, assuming the X-ray source is a point source located at a finite height above the black hole. We fixed i and R_{out} at 70° (Torres et al. 2020) and $3 \times 10^5 r_{\text{g}}$, respectively. The latter value corresponds to the Roche lobe size of the black hole in MAXI J1820, estimated from Kepler’s third law and Equation 4 in Paczyński (1971b), assuming an orbital period of 0.68 day and black hole and companion star masses of $7 M_{\odot}$ and $0.5 M_{\odot}$, respectively (Torres et al. 2020). The model gave $R_{\text{in}} \gtrsim 2 \times 10^4 r_{\text{g}}$ at a 90% confidence limit, with the fit quality $\chi^2/\text{d.o.f.} = 68/137$ comparable to those obtained with the single and double Gaussian models. The lower limit on the innermost radius is consistent with the best-fit value estimated with the double Gaussian model (see above). The best-fit model and the data are shown in Figure 5. The equivalent width of the line is estimated to be 34 ± 6 Å.

4 Discussion

4.1 SED Modeling

We have obtained quasi-simultaneous multiwavelength SED of MAXI J1820 about 60 days after the onset of the first re-brightening phase, covering the near-IR, optical, UV and X-ray bands. We find that the optical-to-X-ray luminosity ratio is much larger than those in the LHS and HSS observed in the initial outburst epoch, as summarized in Table 3. This suggests very different physical conditions of the accretion flow in our epoch compared with these canonical states.

The main part of the optical-to-UV SED can be described by either of the two models: (Model 1) synchro-cyclotron emission by thermal electrons in the RIAF, which is approximated by a

cutoff power-law model, or (Model 2) emission from a truncated hot standard disk, represented by the MCD model. In the following, we show that Model 1 gives a more physically plausible interpretation than Model 2.

4.1.1 RIAF Interpretation (Model 1)

The observed low X-ray luminosity, $L_{\text{pow}}^{\text{X}} \sim 7 \times 10^{32}$ erg s⁻¹, implies a very low mass accretion rate in the inner part of the disk. Then, it is expected that the accretion disk should become RIAF, such as Advection-Dominated Accretion Flow (ADAF; e.g., Narayan & Yi (1995)). Theoretical calculations of ADAF spectra (e.g., Mahadevan (1997); Manmoto et al. (1997)) show that the SED covers a wide range of frequencies over 8 orders of magnitude, consisting of multiple components; the radio-to-optical emission is produced by synchro-cyclotron radiation by hot electrons in the ADAF, whereas the X-ray emission is mainly produced by thermal Bremsstrahlung, with an additional contribution of a Comptonized component of the synchro-cyclotron photons, by the same hot electrons.

To compare our SED with a model prediction, we refer to the theoretical calculation by Manmoto et al. (1997). Their Figure 8 plots a typical SED of ADAF for a black hole mass of $m(\equiv M/M_{\odot}) = 10$ and a normalized mass accretion rate of $\dot{m}(\equiv \dot{M}c^2/8L_{\text{Edd}}) = 10^{-4}$, where L_{Edd} is the Eddington luminosity. It shows a sharp luminosity peak in the optical band and a power-law like spectrum with $\Gamma \simeq 1.8$ in the X-ray band, which are similar to the observed SED. Considering that this ADAF model is a very simplified one (e.g., ignoring outflow), we do not attempt to directly fit the model to our broadband SED, which is beyond the scope of this paper. Instead, we investigate if the main properties of the observed

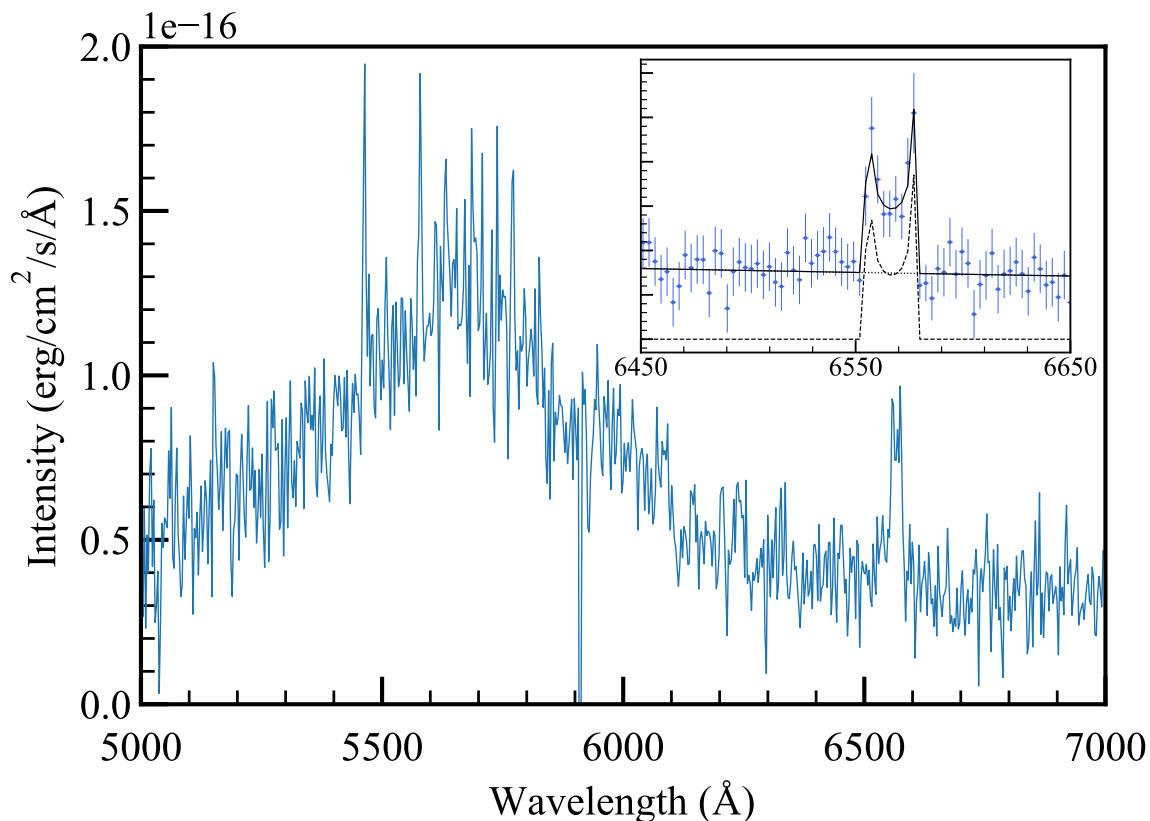


Fig. 5. The Seimei/KOOLS-IFU spectrum of MAXI J1820, taken on 2019 May 11. The magnified image presents the Seimei spectrum around the $H\alpha$ line and the best-fit `diskLine` model.

Table 3. Comparison with the state of MAXI J1820 in each work.

State	MJD	L_X^* (erg sec $^{-1}$)	L_{opt}/L_X^*	Reference
HSS	58314	4×10^{37}	6×10^{-3}	Shidatsu et al. (2019)
LHS	58201	3×10^{37}	4×10^{-2}	Shidatsu et al. (2018)
RIAF	58614	7×10^{32}	8	This work

* L_X and L_{opt} are absorption/extinction corrected luminosity in the 0.5–5 keV and 0.5–5 eV bands, respectively.

SED (peak frequency, optical and X-ray luminosities) can be roughly reproduced by this model only by varying the mass accretion rate. Mahadevan (1997) summarized the scaling laws for ADAF that (1) the luminosity of the synchro-cyclotron radiation $\propto m^{0.5} \dot{m}^{1.5}$, (2) its peak frequency $\nu_P \propto m^{-0.5} \dot{m}^{0.5}$, and (3) the luminosity of the Bremsstrahlung component $\propto m \dot{m}^2$. Thus, if we take $m = 7$ and $\dot{m} = 10^{-3}$, $L_{\text{RIAF}}(0.5\text{--}5\text{ eV}) \sim 1.3 \times 10^{34}$ ergs s $^{-1}$, $\log \nu_P \sim 15$, and $L_{\text{RIAF}}(0.5\text{--}5\text{ keV}) \sim 1.2 \times 10^{32}$ ergs s $^{-1}$ are predicted. These values are all consistent with those of the observed SED ($L_{\text{cpl}} \sim 3 \times 10^{33}$ ergs s $^{-1}$, $\log \nu_P \sim 14.2$, $L_{\text{pow}}^X \sim 7 \times 10^{32}$ ergs s $^{-1}$; see Table 2), within factors of 6, even if we do not apply any tuning for the other parameters (viscosity and magnetic field strength). Thus, the RIAF interpretation is very plausible as the primary origin of the optical and X-ray SED.

4.1.2 Truncated Hot Standard-Disk Interpretation (Model 2)

As an alternative scenario, a major part of the optical SED could be reproduced by optically-thick disk emission. From the best-fit parameters of the MCD component, we are able to estimate the innermost radius of the optically thick disk. For simplicity, here we ignore possible color correction (i.e., the ratio between the color and effective temperatures is assumed to be unity) in deriving the radius. We obtain

$$R_{\text{in}} = 6.3 \times 10^5 \left(\frac{\cos 70^\circ}{\cos i} \right)^{\frac{1}{2}} \frac{D}{3\text{kpc}} \text{km},$$

which corresponds to $1.1 \times 10^4 r_g$ for a black hole mass of $7 M_\odot$. This disk truncation radius is much larger the truncation radius of MAXI J1820 in the LHS estimated by Shidatsu et al. (2018), $12\text{--}36 r_g$. We note that it is even much larger than that observed in the BHXB XTE J1118+480 in its LHS (Chaty 2010), which showed $R_{\text{in}} \sim 350 r_g$.

We estimate the mass accretion rate \dot{M} based on the MCD parameters. Substituting $T_{\text{in}} \sim 5.9 \times 10^{-4}$ keV and $R_{\text{in,SED}} \sim 6.3 \times 10^5$ km into the equation (Kato et al. 2008)

$$\sigma T_{\text{in}}^4 \simeq \frac{3}{8\pi} \frac{GM\dot{M}}{R_{\text{in}}^3},$$

we obtain

$$\dot{m} \sim 0.04(M/7M_{\odot})^{-2}.$$

However, we find that this mass accretion rate is too large to explain the observed optical and X-ray luminosities; assuming that the inner accretion disk is RIAF, its optical and X-ray luminosities are predicted to be 3×10^{36} ergs s⁻¹ and 2×10^{35} ergs s⁻¹, respectively, by using the Manmoto et al. (1997) SED and the scaling laws by Mahadevan (1997) (see Section 4.1.1). Thus, we conclude that the truncated hot standard-disk scenario is unlikely.

4.2 Origin of the Optical-UV Power-Law Component

In addition to the thermal synchro-cyclotron emission from the RIAF and the blackbody from the companion star, a blue power-law component with $\Gamma = 1.4_{-0.9}^{+0.4}$ dominating the UV flux is required from the SED analysis. The slope is consistent with that in the optical band observed in the initial outburst ($\Gamma = 1.7$), which was interpreted to be jet emission (Shidatsu et al. 2018). We thus infer that this optical-UV power-law component is originated from non-thermal synchrotron emission from the jet. Adachi et al. (in prep.) detected rapid variability in the optical band in the same re-brightening phase. The energy spectrum of the variability can be represented with a power law whose slope ($\Gamma \approx 1.2 - 1.5$) is consistent with ours. The presence of the power-law component in the optical SED is consistent with their results. Generally, compact jets are common at low mass accretion rates, when the innermost accretion flow becomes RIAF, including ‘‘hot flow’’ in the LHS.

Although the X-ray spectrum is also well fit with a power-law model with a similar slope, the two power components observed in the optical-UV and X-ray bands do not smoothly connect each other. This indicates that they do not originate from a single component (i.e., synchrotron radiation from the jet). This is in line with our interpretation that the X-ray component mainly originates from the RIAF itself (Section 3.2.2). Nevertheless, we do not rule out the possibility that the same non-thermal electrons in the jets produce X-rays via Comptonization of the synchrotron photons, which may partially contribute to the total X-ray flux.

4.3 Origin of H α Emission Line

We have detected a weak and narrow H α emission line. Similar features are also observed in the quiescence state of dwarf novae (e.g., GW Lib, Hiroi et al. (2009)). The line width of H α

emission constrains the location of its emitting region. We estimate the inner radius to be $\sim 10^5 r_g$ with the double Gaussian model, which is consistent with the lower limit obtained with the `diskline` model ($\gtrsim 2 \times 10^4 r_g$). If the accretion disk were also RIAF at these radii, its temperature would be $\sim 10^7$ K (e.g., Narayan & Yi 1995), which is too high for H α emission to be observed. Hence, we suggest that the entire disk structure cannot be described by a single RIAF solution but cooler material must exist at the outermost region. The H α emission may be originated from an outer disk in the cool state via irradiation by the inner RIAF and jet, or from optically-thin plasma via collisional excitation as discussed in Hiroi et al. (2009). The evolution of the H α profile over the entire outburst epoch will tell us about its origins, which is left as a future work.

5 Summary

We have studied the properties of the accretion disk in the Galactic X-ray black hole binary MAXI J1820 in its first re-brightening phase, on the basis of our quasi-simultaneous near-IR, optical, UV and X-ray observations performed in 2019 May. What we have found can be summarized as follows.

1. The optical-to-X-ray luminosity ratio (~ 8) is found to be much larger than those observed in an earlier outburst epoch when the source was in the LHS or HSS (Shidatsu et al. 2018; Shidatsu et al. 2019), suggesting a very different disk structure.
2. The primary components of the optical and X-ray SED can be best interpreted by a RIAF spectrum, showing a sharp luminosity peak in the optical band (via thermal synchro-cyclotron) and a power-law in the X-ray band (via thermal Bremsstrahlung). By comparison with theoretical calculations, we estimate the mass accretion rate to be $\dot{m} (\equiv \dot{M}c^2/8L_{\text{Edd}}) = 10^{-3}$, which reproduces the observed optical and X-ray luminosities within factors of 6.
3. The truncated hot standard-disk scenario to explain the optical SED is unlikely, because the inferred mass accretion rate would largely overproduce the observed luminosities.
4. In addition to the RIAF emission, a blue power-law component dominating the UV flux is detected. We interpret that this is produced by synchrotron radiation by non-thermal electrons in the jet, as suggested by its rapid variability (Adachi et al. in prep.).
5. The optical spectrum observed with KOOLS-IFU on the Seimei telescope shows a weak H α emission line with an FWHM of $\sim 5.3 \times 10^2$ km s⁻¹. The inner radius of the H α emitting region is constrained to be $\gtrsim 2 \times 10^4 r_g$. We suggest that the entire disk structure cannot be described by a single RIAF solution but cooler material must exist at the outermost region.

Acknowledgments

We thank Kazuya Matsubayashi for his help in the Seimei data reduction. We acknowledge the use of *MAXI* data provided by RIKEN, JAXA and the *MAXI* team, and of public data from the *Swift* data archive. Part of this work was financially supported by Grants-in-Aid for Scientific Research 19K14762 (MS), 17H06362 (YU, HN, NK) from the Ministry of Education, Culture, Sports, Science and Technology (MEXT) of Japan. Optical and Near-Infrared Astronomy Inter-University Cooperation Program, supported by the MEXT of Japan

References

- Atri, P., Miller-Jones, J. C. A., Bahramian, A., et al. 2020, *MNRAS*, 493, L81
- Baglio, M. C., Russell, D. M., & Lewis, F. 2018, *The Astronomer's Telegram*, 11418, 1
- Barden, S. C., ed. 1995, *Society of Photo-Optical Instrumentation Engineers (SPIE) Conference Series*, Vol. 2476, *Fiber Optics in Astronomical Applications*, ed. S. C. Barden, 56–67
- Bernardini, F., Russell, D. M., Shaw, A. W., et al. 2016, *The Astrophysical Journal*, 818, L5
- Bright, J. S., Fender, R. P., Motta, S. E., et al. 2020, *Nature Astronomy*, 4, 697
- Buisson, D. J. K., Fabian, A. C., Barret, D., et al. 2019, *MNRAS*, 490, 1350
- Chambers, K. C., Magnier, E. A., Metcalfe, N., et al. 2016, arXiv e-prints, arXiv:1612.05560
- Chaty, S. 2010, in *American Institute of Physics Conference Series*, Vol. 1314, *International Conference on Binaries: in celebration of Ron Webbink's 65th Birthday*, ed. V. Kalogera & M. van der Sluys, 277–284
- Craine, D. L. C. E. R., ed. 1994, *Society of Photo-Optical Instrumentation Engineers (SPIE) Conference Series*, Vol. 2198, *Instrumentation in Astronomy VIII*, ed. D. L. C. E. R. Craine, 87–97
- . 2010, *Society of Photo-Optical Instrumentation Engineers (SPIE) Conference Series*, Vol. 7733, *Ground-based and Airborne Telescopes III*, ed. D. L. C. E. R. Craine
- Cutri, R. M., Skrutskie, M. F., van Dyk, S., et al. 2003, *2MASS All Sky Catalog of point sources*.
- Denisenko, D. 2018, *The Astronomer's Telegram*, 11400, 1
- Done, C., Gierliński, M., & Kubota, A. 2007, *A&A Rv*, 15, 1
- Ebisawa, K., Makino, F., Mitsuda, K., et al. 1993, *ApJ*, 403, 684
- Esin, A. A., McClintock, J. E., & Narayan, R. 1997, *ApJ*, 489, 865
- Gandhi, P., Rao, A., Johnson, M. A. C., Paice, J. A., & Maccarone, T. J. 2019, *MNRAS*, 485, 2642
- Gierliński, M., Done, C., & Page, K. 2008, *MNRAS*, 388, 753
- . 2009, *MNRAS*, 392, 1106
- Hiroi, K., Moritani, Y., Nogami, D., et al. 2009, *PASJ*, 61, 697
- Ishiguro, M., Takahashi, J., Zenno, T., Tokimasa, N., & Kuroda, T. 2011
- Kato, S., Fukue, J., & Mineshige, S. 2008, *Black-Hole Accretion Disks — Towards a New Paradigm —*
- Kawamuro, T., Negoro, H., Yoneyama, T., et al. 2018, *The Astronomer's Telegram*, 11399, 1
- Kotani, T., Kawai, N., Yanagisawa, K., et al. 2005, *Nuovo Cimento C Geophysics Space Physics C*, 28, 755
- Ma, X., Tao, L., Zhang, S.-N., et al. 2021, *Nature Astronomy*, 5, 94
- Mahadevan, R. 1997, *ApJ*, 477, 585
- Makishima, K., Takahashi, H., Yamada, S., et al. 2008, *PASJ*, 60, 585
- Manmoto, T., Mineshige, S., & Kusunose, M. 1997, *ApJ*, 489, 791
- Markoff, S., Falcke, H., & Fender, R. 2001, *A&A*, 372, L25
- Matsubayashi, K., Ohta, K., Iwamuro, F., et al. 2019, *PASJ*, 71, 102
- Matsuoka, M., Kawasaki, K., Ueno, S., et al. 2009, *Publications of the Astronomical Society of Japan*, 61, 999
- Mihara, T., Nakajima, M., Sugizaki, M., et al. 2011, *PASJ*, 63, S623
- Miller-Jones, J. C. A., Fender, R. P., & Nakar, E. 2006, *MNRAS*, 367, 1432
- Mitsuda, K., Inoue, H., Koyama, K., et al. 1984, *PASJ*, 36, 741
- Nakahira, S., Ebisawa, K., Negoro, H., et al. 2013, *J. Space Sci. Informatics*, 2, 29
- Narayan, R., & Yi, I. 1995, *ApJ*, 452, 710
- Oasa, Y., Ushioda, K., Shibata, Y., et al. 2020, in *Ground-based and Airborne Instrumentation for Astronomy VIII*, Vol. 11447, *International Society for Optics and Photonics*, 114475Z
- Paczyński, B. 1971a, *ARA&A*, 9, 183
- . 1971b, *ARA&A*, 9, 183
- Paice, J. A., Gandhi, P., Shahbaz, T., et al. 2019, *MNRAS*, 490, L62
- Poutanen, J., Veledina, A., Berdyugin, A. V., et al. 2022, *Science*, 375, 874
- Sánchez-Sierras, J., & Muñoz-Darias, T. 2020, *A&A*, 640, L3
- Shakura, N. I., & Sunyaev, R. A. 1973, *A&A*, 500, 33
- Shaw, A. W., Plotkin, R. M., Miller-Jones, J. C. A., et al. 2021, *ApJ*, 907, 34
- Shidatsu, M., Nakahira, S., Murata, K. L., et al. 2019, *ApJ*, 874, 183
- Shidatsu, M., Ueda, Y., Tazaki, F., et al. 2011, *PASJ*, 63, S785
- Shidatsu, M., Ueda, Y., Nakahira, S., et al. 2013, *ApJ*, 779, 26
- Shidatsu, M., Nakahira, S., Yamada, S., et al. 2018, *ApJ*, 868, 54
- Shimokawabe, T., Kawai, N., Kotani, T., et al. 2008, in *American Institute of Physics Conference Series*, Vol. 1000, *Gamma-ray Bursts 2007*, ed. M. Galassi, D. Palmer, & E. Fenimore, 543–546
- Takahashi, J., Zenno, T., & Ishiguro, M. 2013
- Tetarenko, B. E., Shaw, A. W., Manrow, E. R., et al. 2021, *MNRAS*, 501, 3406
- Tetarenko, B. E., Sivakoff, G. R., Heinke, C. O., & Gladstone, J. C. 2016, *ApJS*, 222, 15
- Tomsick, J. A., Yamaoka, K., Corbel, S., et al. 2009, *ApJL*, 707, L87
- Torres, G., Stefanik, R. P., & Latham, D. W. 2019a, *ApJ*, 885, 9
- Torres, M. A. P., Casares, J., Jiménez-Ibarra, F., et al. 2020, *ApJL*, 893, L37
- . 2019b, *ApJL*, 882, L21
- Tucker, M. A., Shappee, B. J., Holoiën, T. W. S., et al. 2018, *ApJL*, 867, L9
- Uttley, P., Gendreau, K., Markwardt, C., et al. 2018, *The Astronomer's Telegram*, 11423, 1
- Veledina, A., Berdyugin, A. V., Kosenkov, I. A., et al. 2019, *A&A*, 623, A75
- Wilms, J., Allen, A., & McCray, R. 2000, *ApJ*, 542, 914
- Yanagisawa, K., Kuroda, D., Yoshida, M., et al. 2010, in *American Institute of Physics Conference Series*, Vol. 1279, *Deciphering the Ancient Universe with Gamma-ray Bursts*, ed. N. Kawai & S. Nagataki, 466–468
- Yatsu, Y., Kawai, N., Shimokawabe, T., et al. 2007, *Physica E Low-Dimensional Systems and Nanostructures*, 40, 434
- Yoshida, M. 2005, *Journal of Korean Astronomical Society*, 38, 117
- You, B., Tuo, Y., Li, C., et al. 2021, *Nature Communications*, 12, 1025
- Zacharias, N., Finch, C. T., Girard, T. M., et al. 2013, *AJ*, 145, 44